STRUCTURAL SCIENCE
CRYSTAL ENGINEERING
MATERIALS

ISSN 2052-5206

Conformational and structural diversity of iridium dimethyl sulfoxide complexes

Benjamin M. Ridgway,[a] Ana Foi,[a] Rodrigo S. Corrêa,[b] Damian E. Bikiel,[a] Javier Ellena,[c] Fabio Doctorovich[a] and Florencia Di Salvo[a]*

[a]Departamento de Química Inorgánica, Analítica y Química Física/INQUIMAE-CONICET, Facultad de Ciencias Exactas y Naturales, Universidad de Buenos Aires, Intendente Güiraldes 2160, Ciudad Universitaria, Pabellón 2, piso 3, Buenos Aires, C1428EGA, Argentina, [b]Departamento de Química, ICEB, Universidade Federal de Ouro Preto, CEP 35400-000, Ouro Preto, MG Brazil, and [c]Instituto de Física de São Carlos, Universidade de São Paulo, Caixa Postal 369, São Carlos, São Paulo 13560-970, Brazil. *Correspondence e-mail: flor@qi.fcen.uba.ar

Received 16 December 2016
Accepted 4 August 2017

Edited by J. Lipkowski, Polish Academy of Sciences, Poland

Keywords: solvent polymorphism; crystal engineering; metallodrug; rotamer.

CCDC references: 1566729; 1566730; 1566731; 1566732

Supporting information: this article has supporting information at journals.iucr.org/b

Transition metal complexes containing dimethyl sulfoxide (DMSO) are important precursors in catalysis and metallodrugs. Understanding the solid-state supramolecular structure is crucial for predicting the properties and biological activity of the material. Several crystalline phases of DMSO-coordinated iridium anions with different cations, potassium (1*a*) and *n*-butylammonium (1*b*), were obtained and their structures determined by X-ray crystallography. Compound (1*a*) is present in two solvatomorphic forms: α and β; the β form contains disordered solvent water. In addition, the structures exhibit different rotamers of the *trans*-$[IrCl_4(DMSO)_2]^-$ anion with the *trans*-DMSO ligands being oriented in *anti* and *gauche* conformations. In consideration of these various conformers, the effects of the crystallized solvent and intermolecular interactions on the conformational preferences of the anion are discussed. In addition, density functional theory calculations were used to investigate the energies of the anions in the different conformations. It was found that hydrogen bonds between water and the DMSO complex stabilize the *gauche* conformation which is the least stable form of the *trans*-DMSO complex. Consequently, by controlling the number of hydrogen-bond donors and acceptors and the amount of water, it may be possible to obtain different solvatomorphs of clinically significant metallodrugs.

1. Introduction

Whereas the molecular structure of a drug is undoubtedly the most important feature determining its function and activity, the supramolecular structure of the bulk solid, including its crystallinity or amorphousness, affects its bioavailability, storage properties, solubility and activity. Increasingly, techniques such as continuous crystallization, co-crystallization and large-scale polymorph screening are being used to find new drug forms, improve drug properties and, contentiously, extend patents on existing drugs (Rossum, 1963; Stromgaard *et al.*, 2009; Nagy & Braatz, 2012; Aaltonen *et al.*, 2009; Ismail *et al.*, 2013; Shan & Zaworotko, 2008). Consequently, an understanding of different crystal forms, whether polymorphs or solvatomorphs, is crucial.

Since the discovery of cisplatin, many metal complexes have been investigated for anticancer activity (Köpf-Maier, 1994; Sava *et al.*, 2011). Unlike other platinum-group metals, iridium complexes were long thought to be less active against cancer cells (Buckley, 1994). However, recent work has shown that careful choice of auxiliary ligands can enable the use of Ir complexes as therapeutic agents (Geldmacher *et al.*, 2012; Leung *et al.*, 2013).

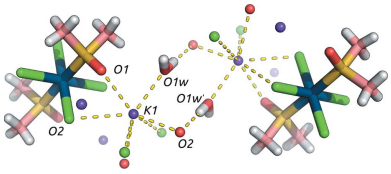

DMSO (dimethyl sulfoxide) is a common solvent used in transition metal chemistry. In addition, DMSO can coordinate to the metal centre, although it is a very labile ligand. This ease of coordination explains its frequent appearance in the single-crystal X-ray structures of many catalytic complexes. Aside from its unexpected appearances, DMSO metal complexes have applications as synthesis precursors. DMSO–metal complexes have also attracted attention because they have been shown to act *in vitro* as potent anticancer agents (Sava *et al.*, 1992; Rademaker-Lakhai *et al.*, 2004). Concerning its behaviour as a ligand, DMSO can coordinate *via* oxygen or sulfur. Early work on divalent metal complexes of DMSO suggested that oxygen coordination was more common, the exception being for Pd complexes, for which sulfur coordination was indicated (Selbin *et al.*, 1961). However, since then, Pd^{II} complexes containing DMSO molecules coordinated through both oxygen and sulfur have been identified (Diao *et al.*, 2012), sometimes in the same crystal (Wayland & Schramm, 1969; Abbasi *et al.*, 2011).

The octahedral *trans*-bis(dimethyl sulfoxide) complex, $[IrCl_4(DMSO)_2]^-$, (1), was first reported by Haddad *et al.* (1974). They reported a pink–orange salt of (1), whose composition was determined by elemental and IR analyses to comprise (1) and a protonated DMSO dimer. They also investigated several other salts of (1) and found various anion geometries. Notably, yellow crystals containing a *cis*-coordinated form were found. Later, James *et al.* determined the structure of the rhodium analogue of (1), which contains protonated DMSO as the countercation or just ion (CSD refcode DMSRHD, $P2/n$; James *et al.*, 1980). Cartwright *et al.* (1988) determined the X-ray crystal structure of (1); for that salt, as with the rhodium analogue determined by James *et al.*, protonated DMSO was found to be the counterion (CSD refcode TAGREY, $P2/c$), forming short proton-bridged DMSO dimeric countercations. Then, a ruthenium analogue of (1) was determined by Alessio *et al.* (1991), and this structure was also found to contain a proton-bridged DMSO dimer. More recently, Messori *et al.* (2003) reported the structure of (1) (CSD refcode TAGREY01, $P2/n$) which is isostructural with the Rh analogues DMSRHD and TAGREY (although TAGREY was solved in $P2/c$).

Concerning the medical applications of metal–DMSO complexes, Cebrián-Losantos *et al.* (2007) determined the structures of several octahedral osmium tetrachloride complexes with various ligands *trans* to a coordinated DMSO ligand. These complexes are salts of pyrazine, triazine, and imidazole derivatives where the nitrogen-containing heterocycle is coordinated *trans*-axially. In addition, they determined the structure of a *trans*-bis(DMSO) complex (CSD refcode VIGKAY, $P\bar{1}$), in which the countercation is also a protonated DMSO dimer, making this osmium complex isostructural with those of the Rh, Ir and Ru complexes (James *et al.*, 1980; Cartwright *et al.*, 1988; Alessio *et al.*, 1991). Furthermore, these osmium complexes show antiproliferative activity against colon and mammary carcinoma cells.

In 2012, Abbasi *et al.* determined the structures of several related potassium ion-mediated coordination polymers (Abbasi *et al.*, 2012). One of these (FANYEA, $P2_1/c$) is a rhodium DMSO complex containing disordered water (0.25 occupation) molecules (Haddad *et al.*, 1974). Interestingly, FANYEA is the only potassium salt of a *trans*-IrL_2Cl_4 (where L is another ligand) anion listed in the CSD, the other structures being either *cis*-anions or ammonium salts. In 1987, James *et al.* determined two polymorphic structures of the diethylammonium salt of the rhodium analogue of (1), both of which formed by the acid hydrolysis of an enamine complex (Gamage *et al.*, 1988).

Here, we report the X-ray crystal structures of several iridium–DMSO complexes, all of which were found to contain sulfur-coordinated DMSO ligands, and we present a different route for the preparation of (1), which is obtained *via* nucleophilic attack of *n*-butylamine on pentachloronitrosyl iridate(III). Using this method, we have obtained crystal structures of two different potassium salts of the *trans*-isomer and an *n*-butylammonium salt, all of which were obtained from the same reaction mixture. Concerning the potassium salts, because these compounds contain the same constituents but exhibit different amounts of crystallized solvent, they are not polymorphs but solvatomorphs, a term that has become popular to describe structures differing only in the number of solvent molecules (Brittain, 2009). We have used single-crystal and powder X-ray diffraction measurements (PXRD) and density functional theory (DFT) calculations to investigate the effect of solvent on the conformation of the *trans*-complexes of (1).

2. Experimental

2.1. Synthesis

$K[IrCl_5NO]$ was purchased from Strem and was purified by recrystallization in dry acetonitrile under an atmosphere of nitrogen. *n*-Butylamine (99.5%) was purchased from Aldrich and used without further purification. DMSO was purchased from Aldrich. $K[IrCl_5(NO)]$ (20 mg, 0.044 mmol) was dissolved in DMSO under a nitrogen atmosphere, forming a dark-brown solution. To this, *n*-butylamine (9.2 µL, 0.092 mmol) was added *via* a syringe, and the solution immediately became a light-orange colour. The solution was stirred for one day even though ^{1}H NMR experiments indicate that the reaction completes in 4 h. Then, a few drops of water were added to the solution and it was left to evaporate. Yellow and yellow–orange crystals began to form after two weeks. The crystals were isolated from solution and inspected under a polarizing microscope and then analysed by single-crystal X-ray diffraction. Several batches of the reaction were studied and in all cases three different solvatomorphs were identified: *trans*-$K[IrCl_4(DMSO)_2]\cdot H_2O$ (1*aα*), *trans*-$K[IrCl_4(DMSO)_2]\cdot 0.25H_2O$ (1*aβ*) and *trans*-$BuNH_3[IrCl_4(DMSO)_2]\cdot 0.5H_2O$ (1*b*). Although the colour of the different solvates was very similar, the crystals of (1*b*) were less cloudy than those of (1*a*). Furthermore, the morphologies were different, tetragonal prisms for (1*a*) and hexagonal crystals for

(1*b*) (see a scheme of the procedure in the supporting information).

2.2. Crystallization experiments under relative humidity controlled atmosphere

Vials containing DMSO solutions of $[IrCl_4(DMSO)_2]^-$ anions were placed in several sealed desiccators with different relative humidities (RH). Then, the samples were left for crystallization. The relative humidity of the closed desiccator was set by using saturated aqueous salt solutions at room temperature, *i.e.* 32% with $CaCl_2{\cdot}6H_2O$, 45% with K_2CO_3, 63% with NH_4NO_3, 86% with KCl, and 95% with $Na_2HPO_4{\cdot}12H_2O$ (Greenspan, 1977). After a few weeks, yellow–orange crystals were obtained in all cases, but single-crystal X-ray diffraction screening showed that the crystalline solvates were identical to those obtained by the crystallization methods described in §2.1 (see a scheme of the procedure in the supporting information).

2.3. Heating experiments

Heating experiments were carried out on the crystals with the aim of exploring possible phase transformations on the loss of water. A crystal of (1*aα*) was mounted on a glass fibre with epoxy resin (Poxipol), and X-ray diffraction measurements were carried out. Then, the crystal, still mounted on the pin, was removed, clamped to a stand and heated with a heat gun. The temperature was monitored using a thermocouple held at the side of the crystal. After five minutes heating at approximately 453 K, the crystal was remounted on the goniometer and a short data collection was carried out. The X-ray diffraction results suggested a single-crystal to single-crystal transformation from the *trans*-$K[IrCl_4(DMSO)_2]{\cdot}H_2O$ to a *cis*-$K[IrCl_4(DMSO)_2]$ (2) complex. Due to the poor quality of data, hydrogen atoms of the water molecules were not assigned or refined (see CIF file and supporting information for details).

2.4. X-ray single-crystal diffraction

Structural data were collected and treated as follows. The crystals were isolated from solution and inspected under a polarizing microscope. Suitable crystals were submerged in vegetable oil and cut down to a size suitable for X-ray diffraction experiments. The samples were mounted in a nylon loop and analysed either at room temperature or under a stream of cooled, dried air at 170 K. X-ray single-crystal diffraction experiments using Mo *Kα* (λ = 0.71073 Å) radiation were carried out using on a Nonius KappaCCD diffractometer and an Oxford Diffraction Gemini E [structure (2) only, see supporting information] diffractometer. A short exploratory data collection was made to assess crystal quality and to determine the unit cell and then, the full data collection was performed. The Oxford Diffraction Gemini E diffractometer [structure (2)] had a generator voltage and current of 50 kV and 40 mA, respectively. The data collection was planned and executed and the data were reduced using *CrysAlisPro* (Agilent, 2013). The Nonius Kappa-CCD diffractometer [structures (1*a*), (1*aβ*) and (1*b*)] had generator voltage and current of 55 kV and 33 mA, respectively. Data collections were made using the *COLLECT* program (Enraf–Nonius, 1997) and the data were reduced using the *DENZO* and *SCALEPACK* programs (Otwinowsky & Minor, 1997) and corrected Lorentz–polarization corrections were made. The data were scaled and merged using *SORTAV* (Blessing, 1995) for (1*aα*) and (1*aβ*). A Gaussian method (Coppens *et al.*, 1965) implemented in *WinGX* (Farrugia, 1999) was used for the absorption correction. Structure solution was carried out using direct methods (*SHELXS*; Sheldrick, 2008). Refinement was performed using full-matrix least squares as implemented in *WinGX* (Farrugia, 1999) and *OLEX*2 (Dolomanov *et al.*, 2009). The CIF was prepared using *SHELXLE* (Hübschle *et al.*, 2011) with *SHELXL*2016 (Sheldrick, 2015).

2.5. Powder diffraction data

Samples were characterized by PXRD using a graphite-filtered Cu *Kα* radiation (λ = 1.5406 Å) on a Siemens D5000 diffractometer.

2.6. Computational details

DFT calculations were made using parallel *ORCA* (version 3.0.2) (Neese, 2012) running on an eight-core AMD desktop computer running *Ubuntu* 14.04 LTS. Dispersion-corrected (Grimme *et al.*, 2011, 2010) geometry optimizations were performed using the B3LYP functional and the Alhrich's def2-SVP basis set (Schäfer *et al.*, 1992, 1994) on all atoms except Ir, which was modelled with the def2-TZVP valence basis set and Stuttgart–Dresden ECP (Weigend & Ahlrichs, 2005; Andrae *et al.*, 1990). ECP parameters implemented in *ORCA* for Ir[SD(60,MWB)] were obtained from the pseudopotential library of the Stuttgart/Cologne group (http://www.theochem.uni-stuttgart.de/pseudopotentials/), whereas ECP basis sets for Ir [DEF2-TZVP] were obtained from the Turbomole basis set library (ftp://ftp.chemie.uni-karlsruhe.de/pub/basen/). Tight SCF convergence criteria were used for geometry optimizations. Coordinate and input file data are available in the supporting information.

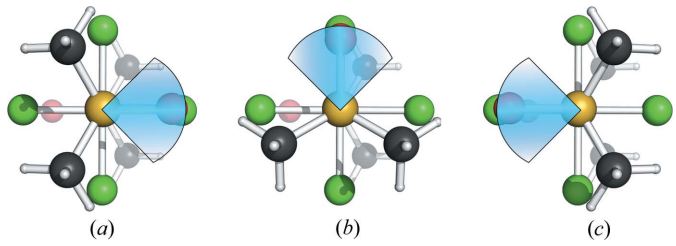

Figure 1
Rotational conformations of the *trans*-anion: (*a*) *anti*, (*b*) *gauche* and (*c*) *syn*. The definition is dependent on the OCCO dihedral angle and independent of rotation of the chloride plane. Colour code: S, yellow; C, black; H, light grey; O, red; Cl, green. Iridium centres are under the sulfur atoms.

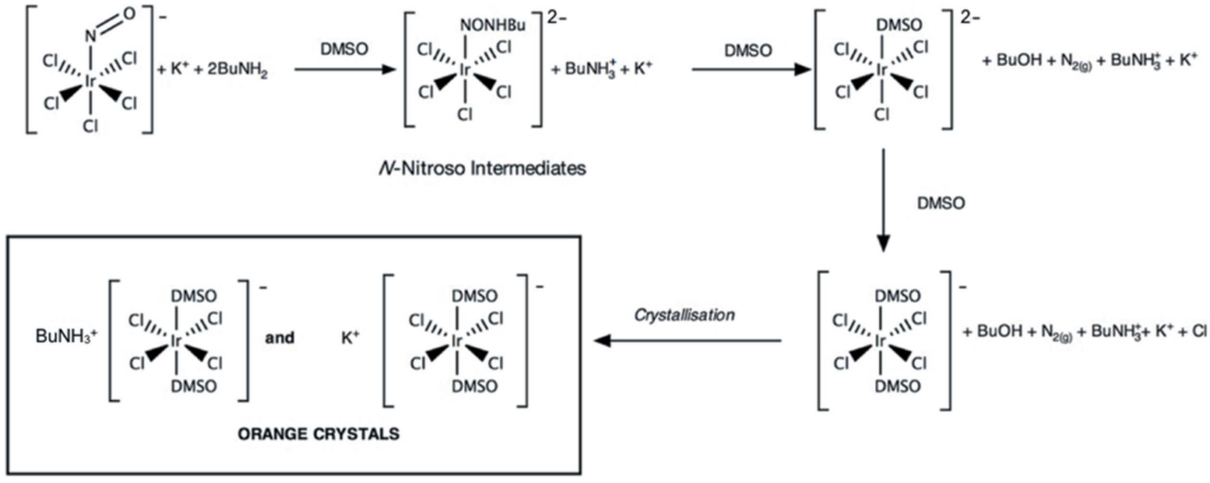

Figure 2
Reaction pathway to obtain (1).

3. Results

Fig. 1 shows the different rotamers found in each crystal structure, and Figs. 2 and 3 summarize the different crystalline forms obtained. Throughout the paper, we refer to the anions by the structure name (1*a*) and (1*b*), solvatomorph type (α and β), and rotamer type (*gauche* and *anti*). In the following text, we define the rotational isomers as *anti*, *gauche* and *syn*, based on the torsion angle made by the S═O bonds of the *trans* DMSO ligands. This labelling scheme and the descriptive angles used are shown in Figs. 1 and S2, respectively. The angles defined in Fig. S2 were used to carry out DFT driver calculations to explore the rotational potential energy surface.

3.1. Formation of *trans*-[$IrCl_4(DMSO)_2$] (1)

The anion (1) was obtained through the reaction of K[$IrCl_5(NO)$] and *n*-butylamine. As illustrated in Fig. 2, one equivalent of the amine attacks the NO bonded to the Ir^{III} and a second equivalent is protonated by the generated proton. Consequently, the first step in this reaction is the formation of a labile *N*-nitroso intermediate; this is then transformed into the corresponding free alcohol after a second nucleophilic attack by a hydroxyl anion generated during the reaction. Finally, the alcohol is lost from the complex and replaced by a solvent molecule, which, in this case, is DMSO (Di Salvo *et al.*, 2008; Doctorovich & Di Salvo, 2007). The complex now contains one DMSO ligand, and this may exert a higher *trans* effect than that of the *N*-nitroso moiety on the *trans*-chloride, resulting in loss of the corresponding chloride and coordination of a DMSO molecule to the metal centre. The *trans*-effect of DMSO ligands is well known; for instance, the *trans*-effect on square-planar platinum complexes containing DMSO has been previously investigated by Kukushkin (1971). DFT calculations indicate that the *trans*-Ir—Cl bond lengthens on the coordination of DMSO (Fig. S3). Thus, the *trans*-DMSO ligand, (1), is formed.

The conversion of the starting complex into $[IrCl_4(DMSO)_2]^-$ in solution was studied using ^{1}H NMR spectroscopy. After 4 h at room temperature, the intermediates disappeared, the alcohol was generated and the ammonium salt formed (Fig. 2). Consequently, in comparison with the previously reported synthesis (Haddad *et al.*, 1974), the desired ion is obtained under mild conditions without the need for concentrated acid.

After leaving the reaction mixture at room temperature and open to the air for two weeks, bright-orange crystals were obtained. The analysis of the resultant material by optical microscope showed two different crystalline forms: hexagonal and tetragonal prisms. Both types of crystal were carefully separated, mounted on a suitable pin (or nylon loop), and analysed using single-crystal X-ray diffraction. Crystallographic data are listed in Table 1. In our initial screening, the tetragonal prisms were found to be potassium salt hydrates of (1) (Fig. 2), whereas the hexagonal crystals were found to comprise the *n*-butylammonium salt (1*b*). Different crystallization experiments were carried but all of them led to the same kind of crystalline material (see *Experimental* for details). Fig. 1 shows the different rotamers found in each crystal structure, and Fig. 3 summarizes the different crystal-

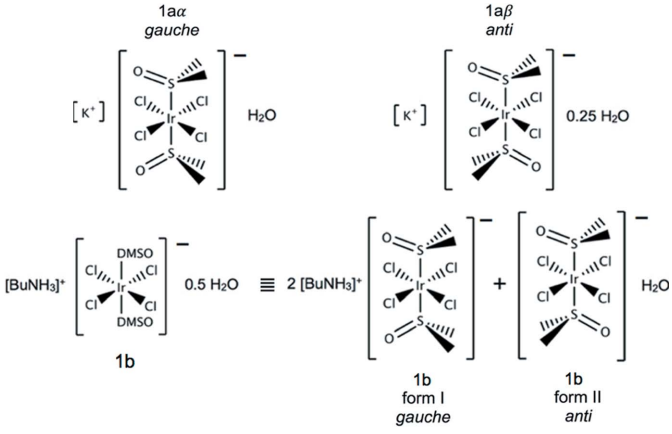

Figure 3
Summary of the crystalline forms and solvatomorphism for (1).

Table 1
X-ray crystal structure data for structures (1*aα*), (1*aβ*) and (1*b*).

	(1*aα*)	(1*aβ*)	(1*b*)
Chemical formula	$C_4H_{12}Cl_4IrO_2S_2{\cdot}K{\cdot}H_2O$	$C_4H_{12}Cl_4IrO_2S_2{\cdot}K{\cdot}0.25(H_2O)$	$C_4H_{12}Cl_4IrO_2S_2{\cdot}C_4H_{12}N{\cdot}0.5(H_2O)$
M_r	547.37	533.86	573.41
Crystal system, space group	Monoclinic, $P2_1/c$	Monoclinic, $P2_1/c$	Monoclinic, $C2/c$
Temperature (K)	293	293	293
a, b, c (Å)	12.1963 (2), 7.4652 (2), 16.4793 (4)	12.7530 (4), 7.8356 (2), 15.3277 (5)	19.8210 (4), 10.0830 (2), 19.5720 (5)
β (°)	96.055 (1)	111.581 (2)	108.657 (2)
V (Å^3)	1492.03 (6)	1424.29 (7)	3706.01 (14)
Z	4	4	8
Radiation type	Mo $K\alpha$	Mo $K\alpha$	Mo $K\alpha$
μ (mm^{-1})	10.21	10.69	8.01
Crystal size (mm)	0.38 × 0.20 × 0.12	0.16 × 0.11 × 0.09	0.21 × 0.12 × 0.11
Diffractometer	KappaCCD	KappaCCD	KappaCCD
Absorption correction	Gaussian (Coppens *et al.*, 1965)	Gaussian (Coppens *et al.*, 1965)	Gaussian (Coppens *et al.*, 1965)
T_{min}, T_{max}	0.064, 0.292	0.134, 0.517	0.263, 0.659
No. of measured, independent and observed [$I > 2\sigma(I)$] reflections	8722, 2614, 2582	8611, 2490, 1781	18983, 3424, 3050
R_{int}	0.061	0.104	0.099
$(\sin\theta/\lambda)_{max}$ (Å^{-1})	0.595	0.595	0.606
$R[F^2 > 2\sigma(F^2)]$, $wR(F^2)$, S	0.030, 0.062, 1.13	0.046, 0.119, 0.95	0.051, 0.132, 1.05
No. of reflections	2614	2490	3424
No. of parameters	141	143	176
H-atom treatment	H-atom parameters constrained	H-atom parameters constrained	H-atom parameters constrained
Weighting scheme	$[w = 1/[\sigma^2(F_o^2) + (0.9117P)^2$ where $P = (F_o^2 + 2F_c^2)/3]$	$w = 1/[\sigma^2(F_o^2) + (0.0507P)^2$ where $P = (F_o^2 + 2F_c^2)/3$	$w = 1/[\sigma^2(F_o^2) + (0.074P)^2 + 31.6594P]$ where $P = (F_o^2 + 2F_c^2)/3$
$\Delta\rho_{max}$, $\Delta\rho_{min}$ (e Å^{-3})	0.70, −0.70	1.73, −2.90	3.53, −1.96

line forms obtained. Throughout the paper, we refer to the anions by the structure name (1*a*) and (1*b*), solvatomorph type (*α* and *β*), and rotamer type (*gauche* and *anti*).

3.2. Potassium *trans*-coordinated salts (1*a*)

Two hydrates of the potassium salt were found, labelled (1*aα*) and (1*aβ*). Both crystallize in the same space group, $P2_1/c$. The unit-cell parameters and Z for both structures are given in Table 1. Bond distances and bond angles for (1*aα*) are given in Table S3 and those for (1*aβ*) are given in Table S4. The asymmetric unit of the (1*aα*)-hydrate contains one water molecule per anion and one *gauche*-DMSO coordinated anion; in contrast, the (1*aβ*)-hydrate contains disordered water. During refinement, the *U*-factor of the water molecule increased; consequently, its occupancy was refined to 0.25 with a reasonable ellipsoid. Because there is neither a clear void space nor a channel through which the solvent can move, the water must be statistically distributed over one in four unit cells. The DMSO ligands are oriented in an *anti*-orientation (Fig. 4). (1*aβ*) contains two half anions in the asymmetric unit, labelled (I) and (II), which both sit on an inversion centre and are, thus, *trans*-*anti*-coordinated. However, the coordinated DMSO ligands have slightly different tilt angles, *i.e.* the O—S—Ir angles for (1*aβ*I) and (1*aβ*II) differ slightly: 115.68 and 115.98°, respectively. The *α* hydrate contains only one crystallographically unique anion; here, the torsion angle is −66.03° and the O—S—Ir tilt angle is 116.02° (Fig. 4*d*).

3.3. *n*-Butylammonium *trans*-coordinated salt (1*b*)

The *n*-butylammonium hydrate, (1*b*), crystallizes in the space group $C2/c$. The unit-cell parameters and Z. The unit-cell parameters and Z are given in Table 1. The bond distances and bond angles are given in Table S2. The unit cell contains two crystallographically unique anions. In each anion, the iridium cation is positioned on a special position: the inversion centre. Thus, the unit cell contains two crystallographically unique half anions, and the two anions have different rotamer configurations. In (1*b*I), the DMSO ligands are *gauche*,

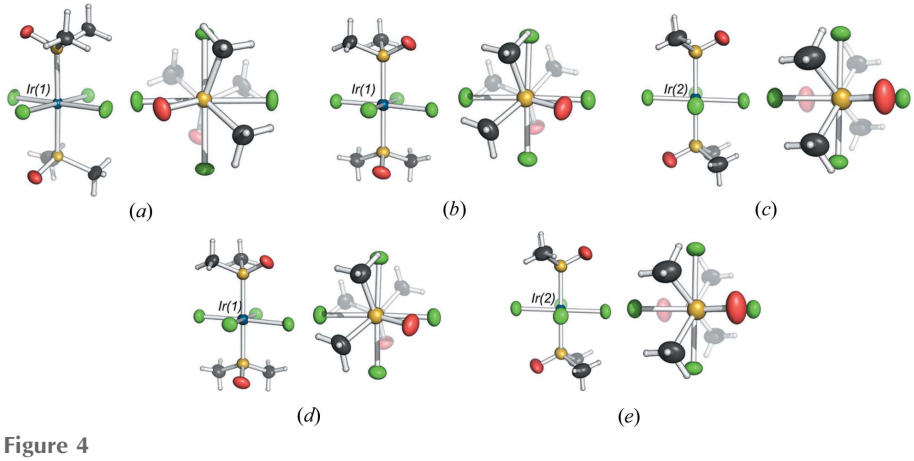

Figure 4
Ellipsoid plots at 50% probability, showing the different rotamers: (*a*) (1*aα*) (*gauche*), (*b*) and (*c*) (1*aβ*) (both *anti*), and (*d*) and (*e*) (1*b*) (I, *gauche*; II, *anti*).

whereas, in (1*b*II), an *anti*-conformation is observed. For (1*b*I) and (1*b*II), the torsion angles are −62.94 and −180°, respectively, and the OSIr angles are 114.61 and 117.09°, respectively. Fig. 4 shows the different anions viewed along the S—Ir—S axis. The crystal structures contain two rotamers of the *trans*-anion: *gauche* and *anti* [(I) and (II) respectively]. The *syn* rotamer was not observed. Furthermore, a search of the CSD for (1) shows that, of *trans* complexes, only *gauche* and *anti* rotamers have been found previously, as shown in Fig. S4, suggesting that the *syn* rotamer is unfavourable.

3.4. Analysis of the relative stability of the *trans*-coordinated rotamers

Relaxed surface scans were carried out at the DFT/B3LYP level of theory using the def2-SVP basis set for the C, H, O and S atoms and the def2-TZVP basis set for the metal. An SDD effective core potential was placed on Ir (see the *Experimental*, Fig. 5 and supporting information for details). The calculations reveal three minima: the *anti*-rotamer being the global minimum energy structure, followed by a slightly higher minimum for the *gauche* structure, and finally, the *syn* rotamer being the highest energy local minimum. The minima are separated by low energy barriers that arise due to the steric clash between the equatorial chloride ligand and the methyl groups of DMSO. However, these barriers are low, approximately 12.5 kJ mol^{-1}, an energy commensurate with that of rotation about a single C—C bond (Yirong, 2011; Smith & Jaffe, 1996). Therefore, as expected, rotation in solution is probably facile and rapid, and deviations from the gas-phase minimum energy structures can be expected to be easily compensated by packing effects and the formation of energetically favourable contacts, such as hydrogen bonds to water molecules and electrostatic interactions with large solvated cations. The DFT optimized structure agrees well with the X-ray crystal structure of DMSO (Thomas *et al.*, 1966), and these differ from the structure of DMSO in the anion mainly by having slightly shorter bond lengths [for example, 1.47 *versus* 1.52 Å in (1β) and the calculated structure, respectively] possibly due to packing effects; indeed, computational studies have shown that significant distortion to bond lengths and bond angles can occur in DMSO because of intermolecular interactions (Mezey & Kapur, 1980). In addition, the pyramidalization of the DMSO molecule is reduced on coordination, as indicated by the increased C—S—C and C—S—O bond angles.

To investigate the importance of the water molecules in the crystal structure and its role with the rotamer stabilization, we attempted to remove water from a crystal by heating. For that experiment we chose a crystal of (1*a*α). On heating, the crystal became slightly opaque and lost its lustre, the surface of the crystal became roughened and its shape became rounded. In the subsequent data collection, the reflections were not sharp and some powder rings were present. Nevertheless, the data were of sufficient quality for structure refinement and the crystal was found to have crystallized in the monoclinic space group $P2_1/n$. To our surprise, the cell parameters were different from those of (1), the crystal structure did not contain water and, more importantly, the iridium complex had changed from *trans* to *cis* geometry [named here as (2)]. To confirm this single-crystal to single-crystal transformation, other crystals of (1*a*α) and (1*a*β) were heated using the procedure outlined above. However, subsequent X-ray analysis showed, despite the poor-quality data, that the crystal structure remained that of the starting compound. We were unable to repeat this transformation in subsequent experiments. DSC experiments performed in (1*a*β) (the main phase) were not conclusive regarding a single-crystal to single-crystal transformation on the bulk. Bulk PXRD measurements show that (1) is the only phase present. Possibly, a crystal of the *cis*-phase grew alongside that of the main phase, (1), and the

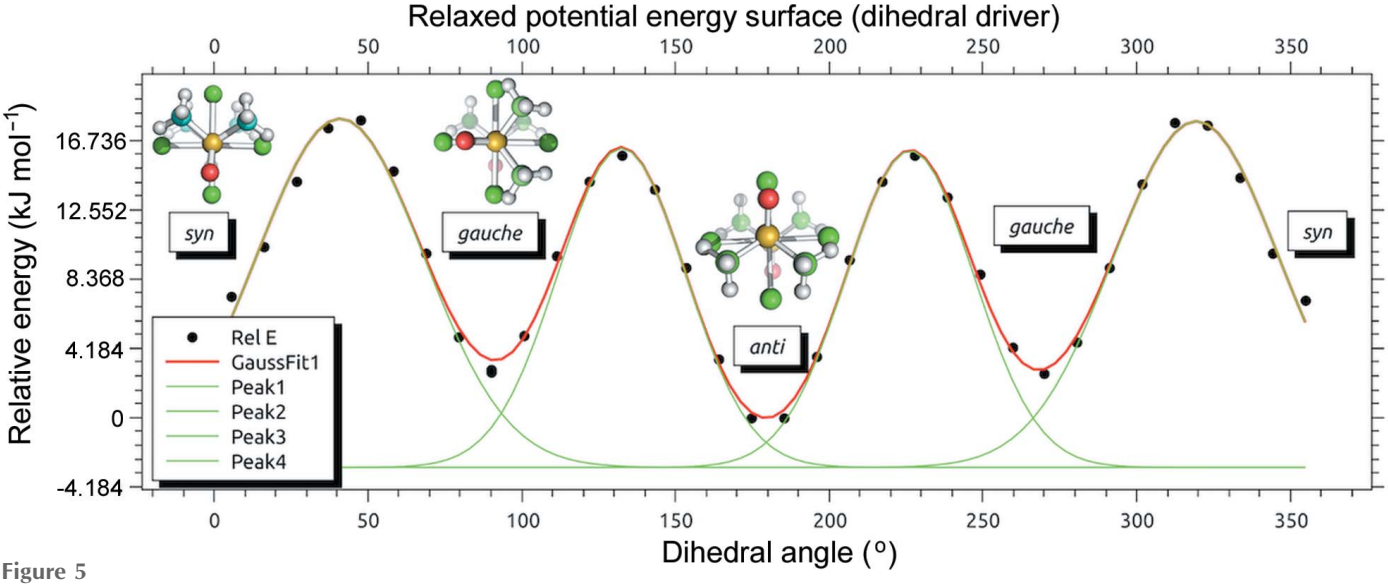

Figure 5
Relaxed potential energy scan. Minima correspond to the *syn*, *anti* and *gauche* conformations, decreasing in energy in that order. Black dots indicate the calculated data points. The green curves are deconvoluted Gaussian curves fitted to the calculated data points. The red curve is the sum of the deconvoluted green Gaussian curves.

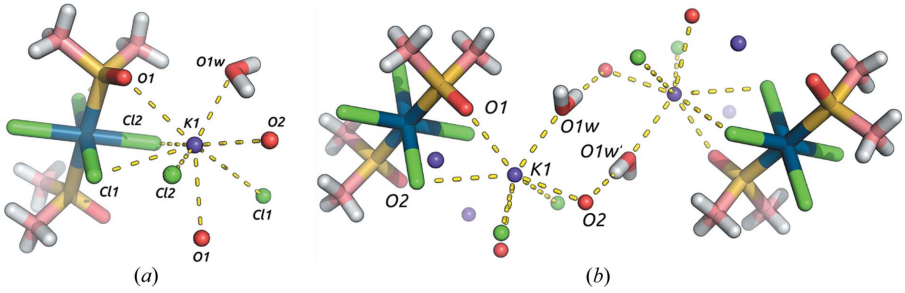

Figure 6
Detail of the (*a*) coordination environment of potassium (K1) in (1*aα*), and (*b*) the centrosymmetric hydrogen-bonded dimer that forms the sheet-like structure shown in Fig. 6(*a*). Not shown are hydrogen bonds from O1*w* (*via* H1*w*) to neighbouring chloride ligands (Cl1 and Cl4).

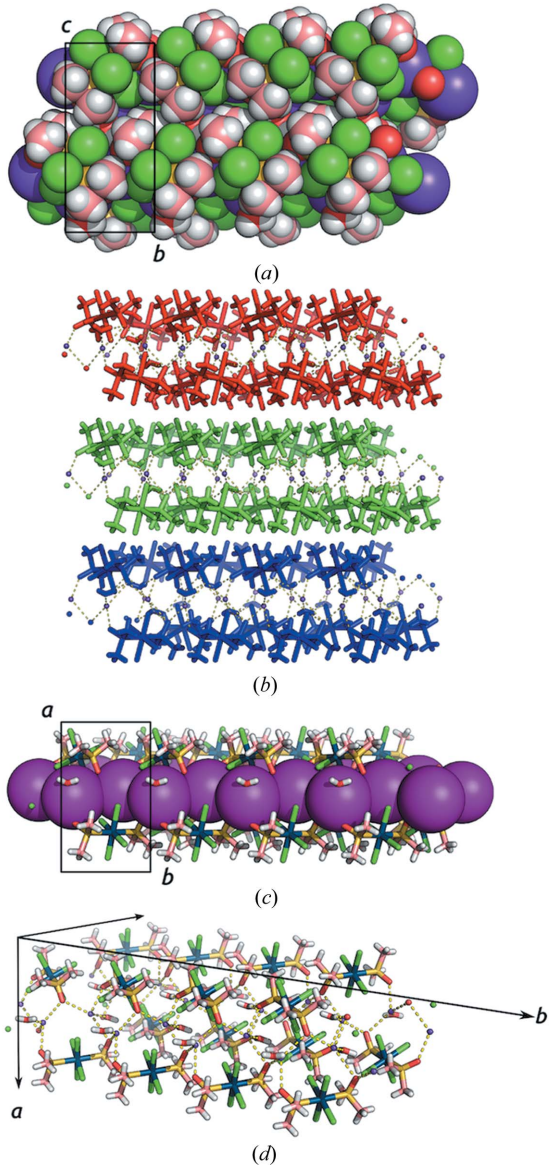

Figure 7
View along the *a* axis of (1*aα*); (*b*) stacking of these sheets along the *a* axis, note the methyl–methyl contacts and methyl–chloride contacts; (*c*) view along the *c* axis showing potassium cations sandwiched between anions; and (*d*) perspective view showing the methyl- and chloride-rich outer layers.

heating of the crystal reduced the crystallinity of the main phase, allowing the *cis*-phase to be detected (Fig. S5).

3.5. Discussion of the supramolecular structures and the role of the hydrogen bond on the rotamer stability

The *α* hydrate of (1*a*) contains one unique anion, and the DMSO ligands are *trans* to each other. In addition, one molecule of water per unit cell is present. This water molecule forms a hydrogen bond with the oxygen atom of the coordinated DMSO ligand. Its molecular structure presents a distorted *gauche* conformation of the DMSO molecules coordinated to the octahedral Ir^{III} centre, as shown in Fig. 6(*a*). The shortest intermolecular interactions in this structure are the hydrogen bonds between water molecules (O1*w*) and oxygen atoms from coordinated DMSO, *i.e.* O2···O1*w* = 2.989 Å and O—H···O = 176.50° (Fig. 6). Hydrogen bonds can be classified as classical and non-classical. Classical hydrogen bonds contain those from donor heteroatoms such as nitrogen, oxygen and halogens. These hydrogen bonds can be further classified as strong, medium or weak. This classification is often made based on the separation between the atoms and the angle made by the *D*—H···*A* hydrogen bond. For common hydrogen bonds, this scheme works reasonably well. However, in very well packed structures, such as those discussed in this paper, it is often difficult to make a clear assessment of the hydrogen-bond energetics (Steiner, 2002). In addition, H1*w* forms an asymmetrically bifurcated hydrogen bond with the chloride ligands of a neighboring iridium complex. Thus, the hydrogen atoms form hydrogen bonds to both Cl1 and Cl4.

Concerning the coordination environment of the potassium cation, K1 is surrounded by eight ligands: one water molecule, three oxygen atoms from two symmetry-related DMSO molecules and four chloride ligands from two symmetry-related complex anions (Fig. 6). The symmetry-related potassium cations are separated by 4.3 Å. A centrosymmetric hydrogen-bonded dimer is formed by the water molecule (O1*w*), which connects the two symmetry-related parts of the dimer through a hydrogen bond to a DMSO oxygen (O1*w*···O2); this DMSO oxygen also forms a contact with the potassium (K1) and the second DMSO oxygen (O1) forms short contacts with potassium only (Fig. 6*b*). Expanding the hydrogen-bonded contacts leads to the formation of a sheet-like structure, as shown in Fig. 7. Fig. 7(*a*) shows the top of this sheet-like structure viewed along the *a* axis. Fig. 7(*c*) shows the side view of the sheet observed along the *c* axis, clearly showing the sandwich-like structure of the anions on the outside and a 'filling' of potassium cations. The exterior surface of the sheet is rich in methyl groups and chloride anions. These sheets stack together, as shown in Fig. 7(*b*), sustained by CH···Cl short contacts.

As in the (1*aα*) crystal structure, (1*aβ*) contains solvent water, a *trans*-anion and a potassium cation. The potassium cation, as for (1*aα*), is octahedrally coordinated (Fig. 8). However, in contrast with the *α*-form, it forms three contacts to oxygen (one from water and two from DMSO) and five close contacts to chloride. Also, the water of crystallization is disordered with an overall occupancy of 25% per water site.

The iridium complex in (1*aα*) crystallized with only one form of the *trans*-isomer, *gauche*; in contrast, the (1*aβ*) form crystallized with two independent anions in the asymmetric unit. Both anions are the *anti*-rotamer, and the iridium atoms sit on an inversion centre. Again, as for the *α*-form, an extended sheet-like structure is observed (similar to Fig. 7*a*) with a core of potassium and chloride anions (similar to Fig. 5*c*). Unlike (1*aα*), because the supramolecular sheets are composed of iridium complexes, an infinite two-dimensional network of K···Cl—Ir—Cl···K contacts is present. In the sheet-like structure, electrostatic interactions between potassium (K1) and the chloride ions of the iridium complex (Cl3, Cl4) form a four-membered cyclic structure. The chain is propagated by the inversion symmetry through Ir2, and the chain continues by contacts through K1 and Cl2 (and the symmetry equivalent of Cl2), forming a second four-membered ring (see Fig. 8 for a close-up of these short contacts). The K···Cl—Ir2—Cl···K chains run along [100], thus forming the sheet-like structure in the (002) plane, as shown in Fig. 9. The distances between K1 and Cl2, Cl2*, Cl3 and Cl4 are 3.229, 3.279, 3.218 and 3.272 Å, respectively. In addition, K1 makes short contacts with O1, O2 and O1*w*, which have separations of 2.826, 2.853 and 3.061 Å, respectively. These layers stack along the *c* axis (Fig. 9) but in (1*aα*), the hydrogen-bonded sheets are quite separated (Fig. 7*b*) with no hydrogen bonds between the sheets. In contrast, for (1*aβ*) the DMSO methyl groups form an interdigitated structure (Fig. 9).

The *n*-butylammonium salt (1*b*) also crystallized with a solvent water molecule of crystallization. The structure, as with (1*aβ*), contains two independent anions. Each of these shows different conformations of DMSO molecules. These are present in the *anti*-conformation and the *gauche*-conformation (Fig. 4). There is a hydrogen-bonded water molecule which has been modelled having a half-occupancy. Unlike the *n*-butylammonium structure determined by us, James' structure [diethylammonium salt of the rhodium analogue of (1)] does not contain water (CSD refcode GEZBOC $P\bar{1}$; Gamage *et al.*, 1988). GEZBOC forms zigzag hydrogen-bonded chains of *trans*-anions linked *via* diethylammonium. The hydrogen bonds are single and formed between the ammonium proton and the DMSO oxygen atom (D_1^1). GEZBOC01 ($P\bar{1}$) also forms hydrogen-bonded zigzag chains, but the hydrogen bonds are bifurcated, forming $R_2^1(5)$ rings (Etter *et al.*, 1990).

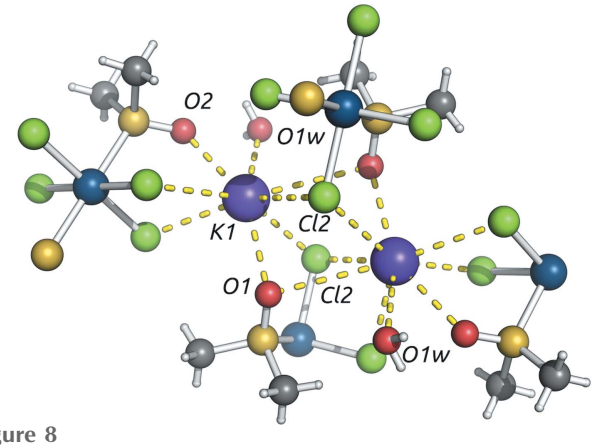

Figure 8
Coordination environment around potassium in (1*aβ*). Only partial anions are shown.

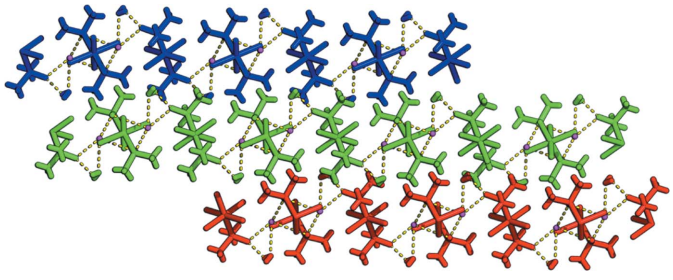

Figure 9
Infinite sheets showing methyl group interdigitation in (1*aβ*). Note the position of the water molecules indicated by pink circles.

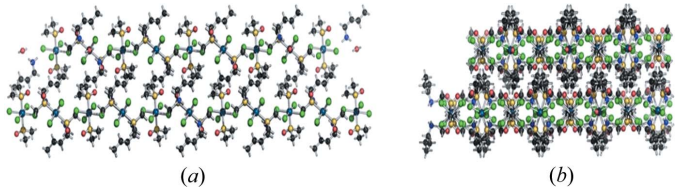

Figure 10
Hydrogen-bonded network in (1*b*) containing $R_1^2(4)$ hydrogen-bonded rings between butylammonium NH and the chloride ligands and $R_1^2(5)$ rings between DMSO oxygen and the butylammonium NH (see Fig. S6 for further details). (*a*) View along the *b* axis and (*b*) the view along [101].

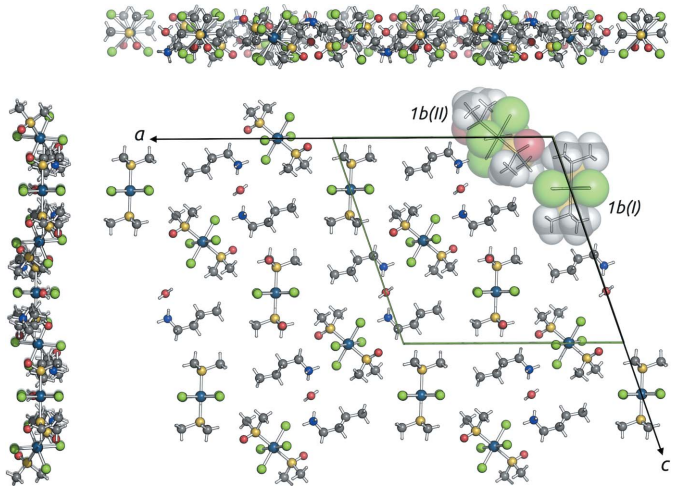

Figure 11
Sheet-like structure in (1*b*). The sheet is shown viewed perpendicular to the *b* axis. The unit cell is shown superimposed. The view along the *c* axis is shown at the top of the image, and that along the *a* axis is shown to the left of the image. Anions (1*b*I) and (1*b*II) are indicated.

Table 2
Cavity volumes occupied by the water of crystallization.

	Complete structure		Water deleted						
	Void volume (%)	Void volume (Å^3)	Void volume (%)	Void volume (Å^3)	'Cavity' size (Å)	Z	Refined occupancy	Volume per water (Å^3)	Volume per asymmetric unit (Å^3)
(1*b*)	2.6	97.98	4.5	166.74	68.74	8	0.5	17.19	8.59
(1*aβ*)	6.4	90.86	9.8	139.7	48.84	4	0.25	12.21	12.21
(1*aα*)	12.1	180.85	15.7	234.23	53.38	4	1	13.35	13.35

n-Butylammonium cations can exist in a variety of conformations, but the linear conformation is the global energy minimum. However, rotations about single bonds are low in energy and in (1*b*), the cation is not linear ($\tau_1 = \tau_2 = 180°$) but has a slightly bent conformation ($\tau_1 = -74.07$ and $\tau_2 = -174.31°$, almost linear). As expected, the *n*-butylammonium cation forms several hydrogen bonds, for example, with a water molecule and the equatorial chloride ligands (Figs. 10 and 11). These hydrogen bonds are listed in the supporting information. Chloride is a good, although non-selective, hydrogen-bond acceptor, and thus an $R_1^2(4)$ graph-set hydrogen-bonded ring is formed (see Fig. S6). Other hydrogen-bonded rings are formed by the water that hydrogen bonds to both the *n*-butylammonium cation and an equatorial chloride, in each type of anion [(1*b*I) and (1*b*II), Fig. S6]. In the *anti*-anion, the four equatorial chlorides interact in pairs with an *n*-butylammonium ion giving place to $R_1^2(4)$ rings as mentioned, and then an N—H···O hydrogen-bond between two cations and a water molecule is observed (Fig. 12). For the *gauche*-anion, two of the four equatorial chlorides interact with two *n*-butylammonium ions and the other two with a molecule of water, which also interacts with the following pair of *n*-butylammonium cations (Fig. 13). As a result, hydrogen-bonded rings $R_4^3(10)$ and $R_2^2(6)$ are observed. The *gauche* form of the anion also results in hydrogen-bonded chains perpendicular to the *a* axis. These again are propagated through the *n*-butylammonium cation and water, forming the column shown in Figs. 13 and 14. These hydrogen bonds propagate to form a two-dimensional hydrogen-bonded sheet in the *ac* plane, shown in Fig. 11. *n*-Butylammonium–water–chloride hydrogen bonds can be seen propagating in the vertical direction in the figure and the chloride–water hydrogen bonds propagate in the horizontal direction. An N—H bond of *n*-butylammonium also forms a hydrogen bond to $O1_{DMSO}$. In addition, there are also several CH···O close contacts, notably C1—H1*A*···O2 and C1—H1*B*···O2, both methyl CH from adjacent coordinated DMSO molecules. Short contacts between C—H···Cl and C—H···O are also present, as listed in Tables S4 and S5.

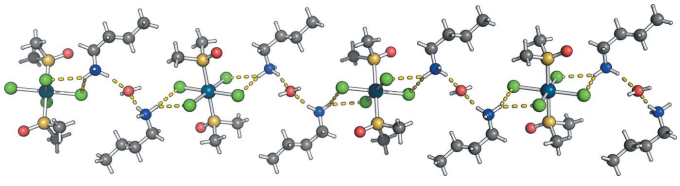

Figure 12
The hydrogen-bonded chain formed between *anti*-anion (1*b*II), *n*-butylammonium and water.

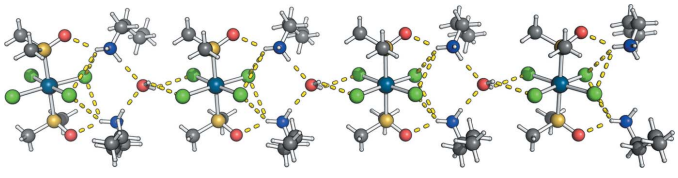

Figure 13
A hydrogen-bonded chain containing the *gauche*-conformer [1*b*I], *n*-butylammonium and water.

3.6. Comparison of the water content of the crystal structures

(1*aα*) contains one water molecule, (1*aβ*) contains 0.25 water molecules. (1*b*), in which the counterion is *n*-butylammonium, has a water molecule with a modelled occupancy of 0.5. In (1*b*), the water molecule forms a common hydrogen-bonding motif, *i.e.* a bifurcated hydrogen bond shared between two chloride ligands of anion (1). To better understand the differences in the water content of these structures, we calculated the volume of the water molecules in these structures, as listed in Table 1. Generally, a water of crystallization occupies about 36 Å^3. Table 2 shows the volume of 'free' space in the structures; the cavity in (1*b*) is small; thus, only half the possible spaces are occupied. (1*aα*) has a larger cavity and has

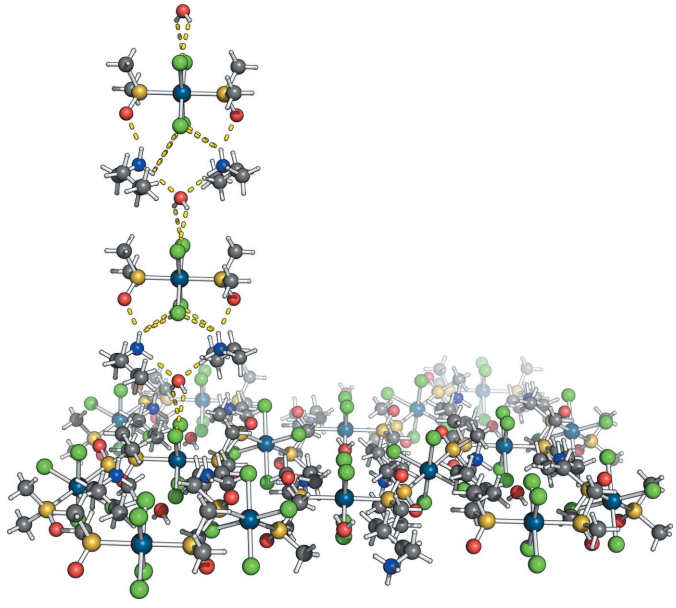

Figure 14
A sheet of hydrogen-bonded (1*b*I) anions. Hydrogen bonds are shown as dashed lines. The hydrogen-bonded column rising from the sheet is the same as that shown in Fig. 13.

an occupancy of one. However, (1*aβ*) has a similar cavity volume to (1*aα*), yet has even lower water occupancy.

The Kitaigorodski packing index is a measure of the packing density of a crystal structure. Molecular crystals typically have packing indices ranging from 65 to 77% (Kitaigorodsky, 1973; van der Sluis & Spek, 1990). However, structures containing voids and disordered solvent may have significantly lower values. The packing indices for these structures are listed in Table S1 and are typical values for molecular crystals. Interestingly, the packing index for the *n*-butylammonium structure is lower than those of the potassium salts, and the packing index of (1*aβ*), which contains disordered water, is high. A possible explanation for the presence of disordered water is that the most energetically favourable packing leaves a small void; this is occupied by water in one out of four asymmetric units, reducing void space but not disrupting the closely packed structure. This structure (1*aα*) may be the kinetic product, where the less energetically favourable *gauche* geometry is stabilized by the presence of a hydrogen bond; in contrast, (1*aβ*) is the thermodynamic product.

To identify the major phase, crystals obtained by slow evaporation of DMSO were screened by selecting each crystal, cutting it to size, mounting the fragment in a nylon loop, and identifying the unit-cell parameters by collecting several frames. The crystals were separated into groups, based on their unit-cell parameters, and we found that most crystals were (1*aβ*) (one-quarter of a molecule of water per asymmetric unit). The crystals were then ground and the PXRD data collected (Fig. S7) show that the only X-ray visible phase is that of (1*aβ*), *i.e.* the other phases must be present, but at such low concentrations that their contribution to diffraction is unobservable.

4. Conclusions

DMSO is a labile ligand that can ligate vacant sites on many metal complexes, yielding precursor compounds that can be converted or metabolized *in vitro* to active metallodrugs. The polymorphic and solvatomorphic behaviour of these complexes is thus of great interest, having consequences for the solubility, bioactivity and storage properties of these compounds. We have described a simple route to obtain complex (1) as potassium and ammonium salts containing different amounts of solvent water. In particular, the two potassium salts include one, (1*aα*), and one-quarter, (1*aβ*), of a water molecule per asymmetric unit. Published structures of *trans*-bis(DMSO) complexes and DFT calculations indicate that the *anti*-conformation is the global minimum energy rotamer, and the bond lengths and bond angles in these compounds are typical, based on previous crystallographic studies and calculations. This occurrence of a less favourable rotamer suggests that the formation of a hydrogen-bonded network mediated by water in (1*aα*) stabilizes the less favourable *gauche*-conformation. However, the most commonly observed structure was that of (1*aβ*); in that structure, the packing index is very high, indicating the optimum use of space and, consequently, the lack of a significant hydrogen-bonding network and the presence of the low-energy *anti*-rotamer. In contrast, (1*b*) has a low packing index, one more typical of wholly organic crystal structures, and contains half a molecule of water per asymmetric unit. Moreover, in (1*b*), both crystallographically independent anions are *anti*, suggesting that at medium packing indices and in the presence of hydrogen-bond donors and acceptors, the *gauche* conformation is stabilized. Furthermore, in the high packing index low water state, the *anti*-conformation dominates and is the dominant structure, whereas in the presence of many hydrogen-bond donors and acceptors (water and *n*-butylammonium), both the low-energy *anti*-rotamer and a *gauche* rotamer are present, and extensive hydrogen bond formation compensates for the less tightly packed structure. These results suggest that, if the number of hydrogen-bond donors and acceptors and the amount of water could be controlled, different solvatomorphs of clinically significant metallodrugs could be obtained.

Funding information

We wish to thank CONICET for a postdoctoral fellowship for BMR and a PhD scholarship for AF. FD, DEB and FDS are CONICET members. The award numbers were PICT2012-1335, UBACYT 2014-2017 GC, No. 20020130100642BA, CNPq, FAPESP and FAPEMIG for funding.

References

Aaltonen, J., Allesø, M., Mirza, S., Koradia, V., Gordon, K. C. & Rantanen, J. (2009). *Eur. J. Pharm. Biopharm.* **71**, 23–37.
Abbasi, A., Geranmayeh, S., Skripkin, M. Y. & Eriksson, L. (2012). *Dalton Trans.* **41**, 850–859.
Abbasi, A., Skripkin, M. Y., Eriksson, L. & Torapava, N. (2011). *Dalton Trans.* **40**, 1111–1118.
Agilent (2013). *CrysAlisPRO*. Agilent Technologies Ltd, Yarnton, Oxfordshire, England.
Alessio, E., Balducci, G., Calligaris, M., Costa, G., Attia, W. M. & Mestroni, G. (1991). *Inorg. Chem.* **30**, 609–618.
Andrae, D., Häussermann, U., Dolg, M., Stoll, H. & Preuss, H. (1990). *Theor. Chim. Acta*, **77**, 123–141.
Blessing, R. H. (1995). *Acta Cryst.* A**51**, 33–38.
Brittain, H. G. (2009). *Polymorphism in Pharmaceutical Solids*, edited by H. G. Brittain. 2nd ed. Boca Raton, FL: CRC Press.
Buckley, R. G. (1994). *Rhodium, Iridium and Palladium Compounds as Experimental Anticancer Drugs*. In *Metal Compounds in Cancer Therapy*, edited by S. P. Fricker, pp. 92–108. Netherlands: Springer.
Cartwright, P. S., Gillard, R. D., Sillanpaa, E. R. J. & Valkonen, J. (1988). *Polyhedron*, **7**, 2143–2148.
Cebrián-Losantos, B. K., Krokhin, A. A., Stepanenko, I. N., Eichinger, R., Jakupec, M. A., Arion, V. B. & Keppler, B. K. (2007). *Inorg. Chem.* **46**, 5023–5033.
Coppens, P., Leiserowitz, L. & Rabinovich, D. (1965). *Acta Cryst.* **18**, 1035–1038.
Diao, T., White, P., Guzei, I. & Stahl, S. S. (2012). *Inorg. Chem.* **51**, 11898–11909.
Di Salvo, F., Estrin, D. A., Leitus, G. & Doctorovich, F. (2008). *Organometallics*, **27**, 1985–1995.
Doctorovich, F. & Di Salvo, F. (2007). *Acc. Chem. Res.* **40**, 985–993.
Dolomanov, O. V., Bourhis, L. J., Gildea, R. J., Howard, J. A. K. & Puschmann, H. (2009). *J. Appl. Cryst.* **42**, 339–341.

Enraf–Nonius (1997). *COLLECT*. Nonius BV, Delft, The Netherlands.
Etter, M. C., MacDonald, J. C. & Bernstein, J. (1990). *Acta Cryst.* B**46**, 256–262.
Farrugia, L. J. (1999). *J. Appl. Cryst.* **32**, 837–838.
Gamage, S. N., James, B. R., Rettig, S. J. & Trotter, J. (1988). *Can. J. Chem.* **66**, 1123–1128.
Geldmacher, Y., Oleszak, M. & Sheldrick, W. S. (2012). *Inorg. Chim. Acta*, **393**, 84–102.
Greenspan, L. J. (1977). *J. Res. Natl. Bur. Stand. Sect. A*, **81A**, 89–96.
Grimme, S., Antony, J., Ehrlich, S. & Krieg, H. (2010). *J. Chem. Phys.* **132**, 154104–154119.
Grimme, S., Ehrlich, S. & Goerigk, L. (2011). *J. Comput. Chem.* **32**, 1456–1465.
Haddad, Y., Henbest, H. & Trocha-Grimshaw, J. (1974). *J. Chem. Soc. Perkin Trans. 1*, pp. 592.
Hübschle, C. B., Sheldrick, G. M. & Dittrich, B. (2011). *J. Appl. Cryst.* **44**, 1281–1284.
Ismail, S. Z., Anderton, C. L., Copley, R., Price, L. S. & Price, L. S. (2013). *Cryst. Growth Des.* **13**, 2396–2406.
James, B. R., Morris, R. H., Einsten, F. W. B. & Willis, A. (1980). *J. Chem. Soc. Chem. Commun.* pp. 31.
Kitaigorodsky, A. (2012). *Moecular Crystals and Molecules*. New York: Academic Press.
Köpf-Maier, P. (1994). *Eur. J. Clin. Pharmacol.* **47**, 1–16.
Kukushkin, Y. N. (1971). *Chem. Pap.* **25**, 380–384.
Leung, C. H., Zhong, H. J., Chan, D. S. & Ma, D. L. (2013). *Coord. Chem. Rev.* **257**, 1764–1776.
Messori, L., Marcon, G., Orioli, P., Fontani, M., Zanello, P., Bergamo, A., Sava, G. & Mura, P. (2003). *J. Inorg. Biochem.* **95**, 37–46.
Mezey, P. G. & Kapur, A. (1980). *Can. J. Chem.* **58**, 559–566.
Nagy, Z. K. & Braatz, R. D. (2012). *Annu. Rev. Chem. Biomol. Eng.* **3**, 55–75.
Neese, F. (2012). *Wiley Interdiscip. Rev.: Comput. Mol. Sci.* **2**, 73–78.
Otwinowski, Z. & Minor, W. (1997). *Methods Enzymol.* **276**, 307–326.
Rademaker-Lakhai, J. M., van den Bongard, D., Pluim, D., Beijnen, J. H. & Schellens, J. H. (2004). *Clin. Cancer Res.* **10**, 3717–3727.
Rossum, J. van (1963). *J. Pharm. Pharmacol.* **15**, 285–316.
Sava, G., Bergamo, A. & Dyson, P. J. (2011). *Dalton Trans.* **40**, 9069–9075.
Sava, G., Pacor, S., Mestroni, G. & Alessio, E. (1992). *Clin. Exp. Metastasis*, **10**, 273–280.
Schäfer, A., Horn, H. & Ahlrichs, R. (1992). *J. Chem. Phys.* **97**, 2571–2577.
Schäfer, A., Huber, C. & Ahlrichs, R. (1994). *J. Chem. Phys.* **100**, 5829–5835.
Selbin, J. W., Bull, W. E. & Holmes, L. H. Jr (1961). *J. Inorg. Nucl. Chem.* **16**, 219–224.
Shan, N. & Zaworotko, M. J. (2008). *Drug Discov. Today*, **13**, 440–446.
Sheldrick, G. M. (2008). *Acta Cryst.* A**64**, 112–122.
Sheldrick, G. M. (2015). *Acta Cryst.* C**71**, 3–8.
Sluis, P. van der & Spek, A. L. (1990). *Acta Cryst.* A**46**, 194–201.
Smith, G. D. & Jaffe, R. L. (1996). *J. Phys. Chem.* **100**, 18718–18724.
Steiner, T. (2002). *Angew. Chem. Int. Ed.* **41**, 48–76.
Stromgaard, K., Krogsgaard-Larsen, P. & Madsen, U. (2009). Editors. *Textbook of Drug Design and Discovery*. p. 49, Boca Raton: CRC Press.
Thomas, R., Shoemaker, C. B. & Eriks, K. (1966). *Acta Cryst.* **21**, 12–20.
Wayland, B. B. & Schramm, R. F. (1969). *Inorg. Chem.* **8**, 971–976.
Weigend, F. & Ahlrichs, R. (2005). *Phys. Chem. Chem. Phys.* **7**, 3297–3305.
Yirong, M. (2011). *Comput. Mol. Sci.* **1**, 164–171.